



Cite this: *RSC Adv.*, 2020, 10, 620

Received 14th October 2019
Accepted 20th December 2019

DOI: 10.1039/c9ra08402a

rsc.li/rsc-advances

Suppressing H₂ evolution by using a hydrogel for reversible Na storage in Na₃V₂(PO₄)₃

Xianying Fan, Xiaoyu Gao, Xuan Zhang, Guijia Cui, Huichao Lu, Zhixin Xu and Jun Yang *

We report a low-cost hydrogel electrolyte by adding 3 wt% poly(acrylate sodium) (PAAS) into 1 M Na₂SO₄ aqueous electrolyte, which achieves a widened electrochemical stability window (ESW) of 2.45 V on stainless steel current collector from 2.12 V in 1 M Na₂SO₄ aqueous electrolytes (AE). Moreover, the H₂ evolution potential reaches −1.75 V vs. Ag/AgCl on titanium current collector. The results reveal that the polymer network structure of PAAS has the ability to interact with water molecules and thus the hydrogen evolution reaction can be limited effectively, which broadens the ESW of aqueous electrolyte and allows the reversible Na-ion intercalation/deintercalation of Na₃V₂(PO₄)₃ as an anode material in aqueous electrolyte reported for the first time.

Introduction

Sodium-ion batteries have attracted much attention in the field of energy storage systems due to the rich abundance and low cost of sodium. Nonetheless, conventional sodium-ion batteries are based on toxic and flammable organic electrolytes which may cause security issues in practical applications.^{1–5} Aqueous electrolytes for sodium-ion batteries have the advantages of non-flammability, high ionic conductivity, and low cost. However, the thermodynamic ESW of water as an electrolyte solvent is restricted to barely 1.23 V arising from the H₂ and O₂ evolution, and thus the output voltage and energy density of cells are limited.^{5–14} Recently, Wang *et al.*⁸ and Battaglia *et al.*⁹ have made remarkable progress on high concentration (9.26 M) sodium trifluoromethanesulfonate (NaCF₃SO₃) and ultrahigh (up to 37 M) concentration sodium bis(fluorosulfonyl)imide (NaFSI) in water by forming “water-in-salt” electrolyte (WiSE), which has been the most effective approach to bind “free” water for extending stable electrochemical windows to more than 2.5 V. But the exorbitant cost due to the massive use of organic sodium salts and temperature-dependent solubility of salts hinder the practical application of the WiSE strategy. Therefore, a simple and economical strategy to suppress the electrochemical decomposition of water for aqueous sodium batteries is of great importance.

Besides, it is also meaningful to select an electrode material that is compatible with the electrolytes to achieve Na-ion storage. Nowadays, the often used anode materials, such as activated carbon (2–2.6 V vs. Na/Na⁺),¹⁵ NaTi₂(PO₄)₃ (2.1 V vs. Na/

Na⁺),¹⁶ vanadium oxide Na₂V₆O₁₆·*n*H₂O (2.5 V vs. Na/Na⁺),¹² or organic anodes polyimide (2.2–2.4 V vs. Na/Na⁺),^{17,18} possess relatively high electrode potentials in aqueous sodium-ion batteries, which leads to low cell voltage output. Na₃V₂(PO₄)₃ with a NASICON structure has been intensively investigated for sodium-ion batteries as a cathode.^{19–24} In fact, Na₃V₂(PO₄)₃ has the characteristics of dual potential plateaus at 3.4 V vs. Na⁺/Na and 1.6 V vs. Na⁺/Na, and the lower one has been utilized for anode use in Na₃V₂(PO₄)₃ symmetrical full cells with non-aqueous electrolytes that show good cycle stability and high rate capability.^{23,24} Provided Na₃V₂(PO₄)₃ could be also used anode in aqueous electrolytes, a higher cell voltage can be expected. However, since its Na⁺-intercalation potential (1.6 V vs. Na/Na⁺) is much lower than hydrogen evolution potential (2.3 V vs. Na/Na⁺),⁵ finding a special aqueous electrolyte that fits Na₃V₂(PO₄)₃ anode is important.

Herein, we introduce a new aqueous electrolyte based on the combination of inexpensive Na₂SO₄ salt and hydrogel poly(acrylate sodium) (PAAS). The interaction among salt, PAAS and water molecules suppresses hydrogen evolution reaction effectively, which broadens the ESW of aqueous electrolyte and allows the reversible Na-ion intercalation/deintercalation of Na₃V₂(PO₄)₃ as an anode in aqueous electrolyte.

Results and discussion

Hydrogel electrolytes (HEs) of various concentrations were prepared by mixing 1 M Na₂SO₄ aqueous electrolytes with an appropriate amount of PAAS (1, 3, 5 wt% respectively, which are noted as HE-1, HE-3, HE-5, *M_w* = 300w–700w, Aladdin), and then by intense stirring at room temperature until dissolved. As shown in Fig. 1a and b, the states of the electrolytes changes from liquid to gel after the addition of PAAS, and the viscosity of

Shanghai Electrochemical Energy Devices Research Center, Department of Chemical Engineering, Shanghai Jiao Tong University, Shanghai 200240, China. E-mail: yangj723@sjtu.edu.cn



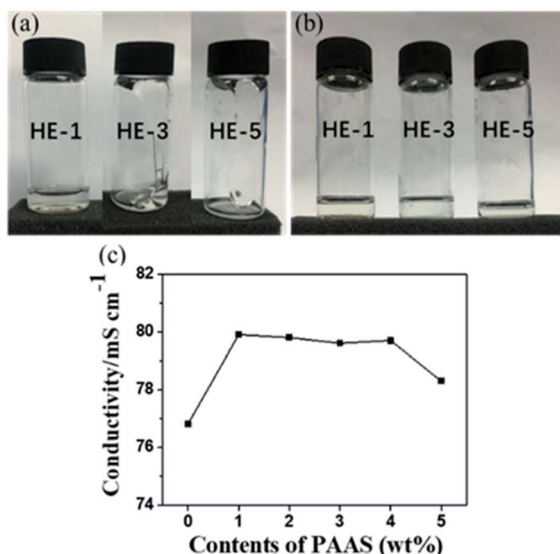


Fig. 1 Physical states and conductivities of the electrolytes. The appearances of HEs after flipping the vials for 2 s (a) and for 60 s (b). The conductivities of AE and HEs (c).

the weakly acidic HEs (pH = 5.5–7) increases with higher PAAS content. The conductivity of HEs at room temperature is about 78–80 mS cm⁻¹ compared to 76 mS cm⁻¹ for AE (Fig. 1c). The higher conductivity with PAAS might be mainly related to the increased Na⁺ content from PAAS. The declined conductivity for 5 wt% PAAS could be explained by the rising viscosity. It is noteworthy that the conductivity of the aqueous gel polymer electrolytes is much higher than those of the organic sodium-ion electrolytes (6–12 mS cm⁻¹) and most of “water-in-salt” electrolytes (~10 mS cm⁻¹).^{5,8,9}

Fig. 2 shows the ESW of HEs obtained by potential dynamic polarization using a stainless steel (SS) working electrode in a three-electrode cell. The addition of various amounts of PAAS to the AE results in different degrees of ESW broadening and the content of 3 wt% PAAS (HE-3) exerts the strongest effect. Using HE-3, there is a sharp over-potential increase of about 330 mV for H₂ evolution reaction (HER). That is, the initial HER potential shifts from -0.98 V for AE to -1.31 V vs. Ag/AgCl for HE-3, and the total ESW is as wide as 2.45 V compared to 2.12 V in AE. It may be ascribed to the strong water absorption effect of PAAS which causes self-ionizing H⁺ of water molecules to interact with -COO⁻, resulting in a decrease in the mobility of H⁺ in HEs and negative shift of the hydrogen evolution potential.

To better explain the function of PAAS in 1 M Na₂SO₄ aqueous electrolyte, we have used DMol3 method based on density functional theory (DFT)^{25,26} to calculate the binding energy, and determine the possible combined forms of Na⁺ and oxygen atoms with water molecules in the cluster. The results of the binding energy changes among PAAS, Na₂SO₄ and water molecules are provided in Fig. 3a. The binding energy between the above three is -0.69 eV (<0), which indicates that PAAS and Na₂SO₄ have some interaction with water molecules in HEs. This may be due to the similar attraction effect between -COO⁻

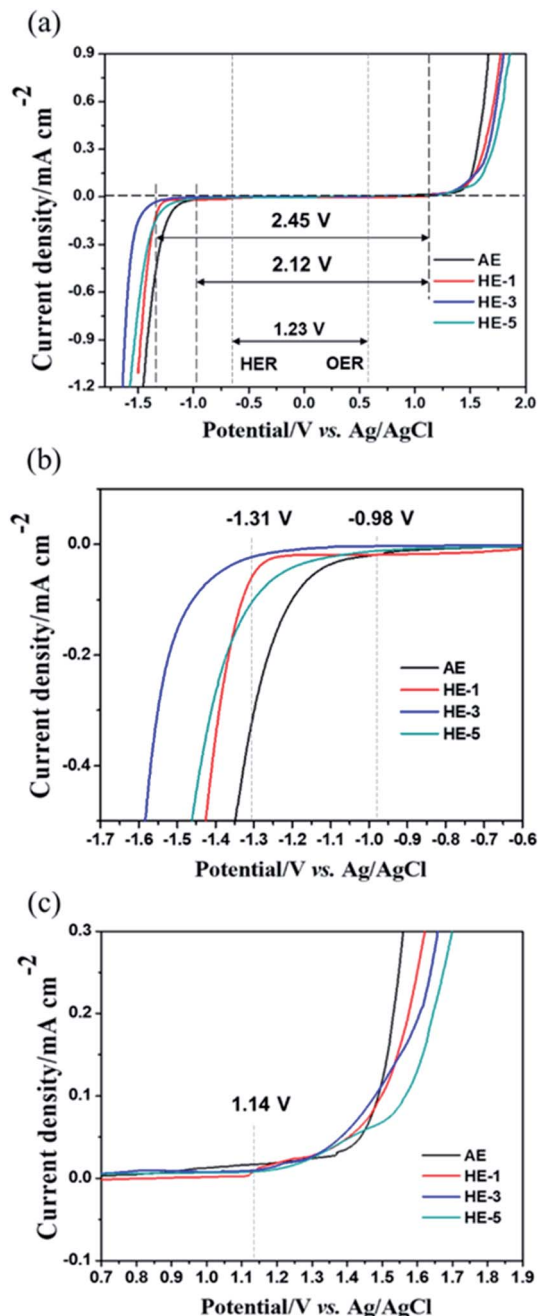


Fig. 2 Potentiodynamic scan of electrolytes on a stainless-steel working electrode. The electrochemical stability windows of AE and HEs, scan rate: 10 mV s⁻¹. (a) The enlarged regions near anodic and cathodic extremes of the electrochemical stability windows on stainless steel current collector (b) and (c).

or SO₄²⁻ to Na⁺ that makes PAAS and Na₂SO₄ preferentially form a more structurally stable molecular cluster to restrain the water molecule tightly. Na⁺ ions from both PAAS and the Na₂SO₄ have solvation with water molecules and the remaining unsolvated water molecules act with the carboxylate in a manner to form hydrogen bonds (Fig. 3a and b, W1–W7 and Table 1). Moreover, the widened ESW may be also related to the interaction of ion-pair charges between -COOH groups, which are



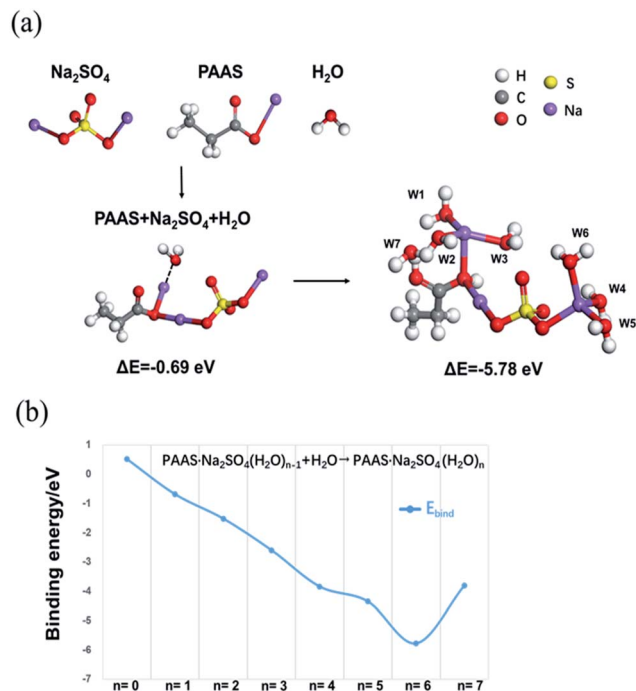


Fig. 3 Relative binding energies at 298 K of PAAS, Na_2SO_4 and H_2O from DFT calculations using Dmol3 model (a). Binding energies (E_{bind}) for the Na^+ cation to approach multiple water molecules ($n = 0-7$) as calculated by DFT calculations with Dmol3 model (b).

formed by self-ionizing H^+ and $-\text{COO}^-$ groups. The charge interaction between ions expands the polymer network and causes a large osmotic pressure, which enhances the interaction between water molecules and oxygen atoms and also raises salt tolerance ability of PAAS²⁷ at the same time. Since the part of H^+ exists in the form of a $-\text{COOH}$ group, the reduction resistance of the water molecules is slightly enhanced. These interactions jointly lead to the improvement in cathodic stability observed in HEs as shown in Fig. 2b.

Fig. 4a shows the Fourier transform infrared (FTIR) analysis of PAAS, Na_2SO_4 and water molecules. The strong peak at 1124 cm^{-1} shown in AE and HEs can be attributed to the anti-symmetric stretching vibration of SO_4^{2-} . For PAAS, the peak at

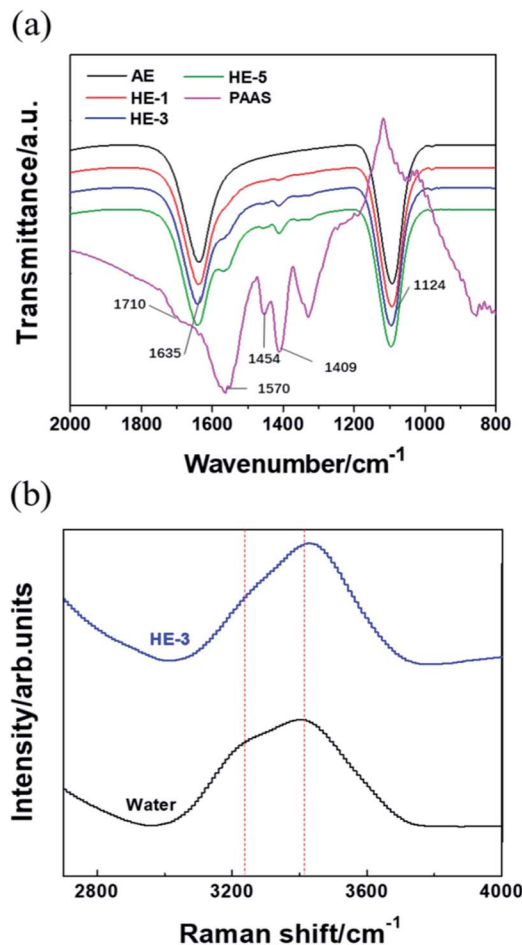


Fig. 4 FTIR spectra of PAAS, HEs and AE (a). Raman spectra of HE-3 and pure water (b).

1454 cm^{-1} indicates the angle vibration absorption of $-\text{CH}_2$, while the peaks at 1570 and 1409 cm^{-1} correspond to the antisymmetric and symmetric stretching vibration absorption peaks of $-\text{COO}^-$, respectively. These three characteristic peaks become more pronounced with the increase of PAAS content. The stretching vibration absorption peak of $\text{C}=\text{O}$ (1710 cm^{-1}) disappears when PAAS is added into aqueous solutions, indicating that the combination of the water molecules with carboxylate oxygen may weaken the $\text{C}=\text{O}$ stretching vibration absorption peak. Besides, the $\text{H}-\text{O}-\text{H}$ bending vibration is red-shifted from 1630 cm^{-1} to 1635 cm^{-1} when the concentration of PAAS increased from 0% (AE) to 5 wt% (HE-5), which is likely due to an increase of viscosity.

It can be observed in Fig. 4b that HE-3 shows a narrower peak compared to the broad Raman band from 3000 cm^{-1} to 3700 cm^{-1} of pure water. In addition, the intensity of the peak at 3200 cm^{-1} corresponding to free water is lower and the peak of coordinated water shifts to 3550 cm^{-1} from 3410 cm^{-1} . Hence, it can be inferred that HE-3 can achieve better electrochemical stability due to the combination of a fraction of water molecules.

Table 1 Relative energies of $\text{PAAS}\cdot\text{Na}_2\text{SO}_4(\text{H}_2\text{O})_n$ ($n = 1-7$) clusters as calculated by DFT calculations with Dmol3 model

Molecules	E [Ha]	ΔE [Ha]	ΔE [eV]
$\text{C}_2\text{H}_5\text{COONa}$	-427.206724	—	—
Na_2SO_4	-1018.656642	—	—
H_2O	-75.861179	—	—
$\text{C}_2\text{H}_5\text{-COONa}\cdot\text{Na}_2\text{SO}_4\cdot\text{H}_2\text{O}$ (W1)	-1521.749738	-0.025193	-0.69
$\text{C}_2\text{H}_5\text{-COONa}\cdot\text{Na}_2\text{SO}_4\cdot 2\text{H}_2\text{O}$ (W2)	-1597.641585	-0.055861	-1.52
$\text{C}_2\text{H}_5\text{-COONa}\cdot\text{Na}_2\text{SO}_4\cdot 3\text{H}_2\text{O}$ (W3)	-1673.542468	-0.095565	-2.60
$\text{C}_2\text{H}_5\text{-COONa}\cdot\text{Na}_2\text{SO}_4\cdot 4\text{H}_2\text{O}$ (W4)	-1749.449321	-0.141239	-3.84
$\text{C}_2\text{H}_5\text{-COONa}\cdot\text{Na}_2\text{SO}_4\cdot 5\text{H}_2\text{O}$ (W5)	-1825.329216	-0.159955	-4.35
$\text{C}_2\text{H}_5\text{-COONa}\cdot\text{Na}_2\text{SO}_4\cdot 6\text{H}_2\text{O}$ (W6)	-1901.242812	-0.212372	-5.78
$\text{C}_2\text{H}_5\text{-COONa}\cdot\text{Na}_2\text{SO}_4\cdot 7\text{H}_2\text{O}$ (W7)	-1977.031559	-0.13994	-3.81



The material type of the anode current collector has an apparent influence on the HER over-potential. We further measured the ESW of HE-3 by potentiodynamic scanning on different metal electrodes, including stainless steel (SS), Al, Ti and Pt (Fig. 5a). Al is a typical current collector and can suppress the HER potential to -1.55 V vs. Ag/AgCl compared with Pt (-1.0 V) or SS (-1.31 V). Furthermore, the HER potential for Ti electrode can reach -1.75 V (vs. Ag/AgCl) in HE-3. The HER over-potential of the anode current collectors in HE-3 follows the sequence: Ti > Al > SS > Pt.

The electrode materials that have been reported in aqueous electrolyte systems are shown in Fig. 5b. The widened ESW of HE-3 provides more options for electrode materials available for reversible sodium-ion storage. We have selected NASICON structured $\text{Na}_3\text{V}_2(\text{PO}_4)_3$ material for a potential Na^+ intercalation electrode with titanium current collector. The synthesized $\text{Na}_3\text{V}_2(\text{PO}_4)_3$ has irregular particle shapes in the sizes mostly below $5\ \mu\text{m}$ (Fig. 6a and b). Its XRD pattern in Fig. 6c accords with the standard one well. TG result indicates that the $\text{Na}_3\text{V}_2(\text{PO}_4)_3$ material contains 4.44% carbon (Fig. 6d), and the weight increases after $550\ ^\circ\text{C}$ could be attributed to the oxidation of V^{3+} in $\text{Na}_3\text{V}_2(\text{PO}_4)_3$.^{21,22} Fig. 5c shows cyclic voltammograms of $\text{Na}_3\text{V}_2(\text{PO}_4)_3$ electrode in the three-electrode system containing HEs and AE at a scan rate of $5\ \text{mV s}^{-1}$. As evidenced by the results in Fig. 5c, the intercalation of sodium-ion in $\text{Na}_3\text{V}_2(\text{PO}_4)_3$ electrode is accompanied by hydrogen evolution

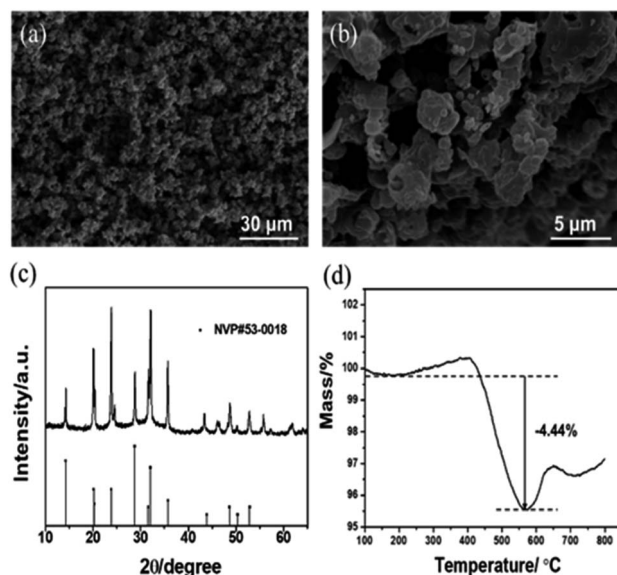


Fig. 6 SEM images (a and b), XRD pattern (c) and TG curve (d) of the as-prepared $\text{Na}_3\text{V}_2(\text{PO}_4)_3$.

reaction in AE, HE-1 and HE-5. Due to the strong competing reduction, no obvious Na^+ deintercalation peak can be observed in AE. On the other hand, although the Na^+ intercalation and

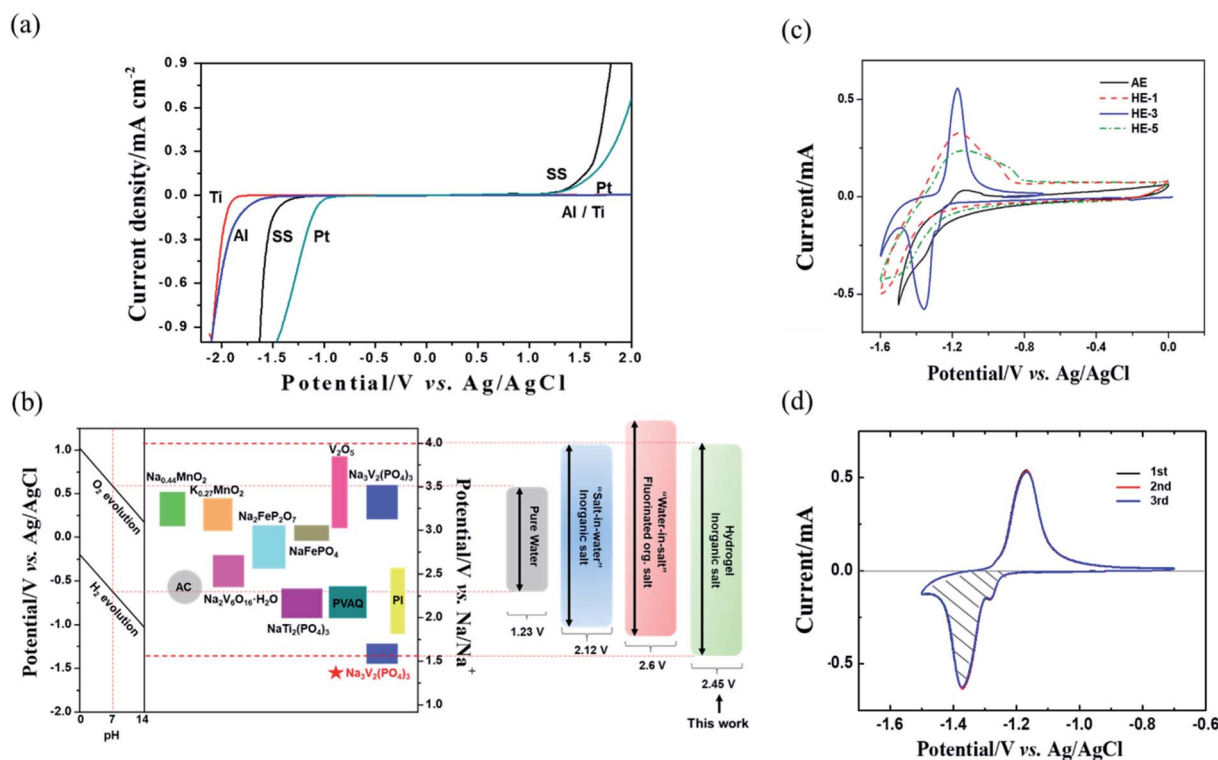


Fig. 5 The electrochemical stability windows of HE-3 on different working electrodes, scan rate: $10\ \text{mV s}^{-1}$ (a). The intercalation potential of some electrode materials that could possibly be employed for aqueous sodium-ion storages and comparison of aqueous sodium-ion storages end-of-charge voltages with various salts (b). CV of $\text{Na}_3\text{V}_2(\text{PO}_4)_3$ working electrode (coated on titanium) in a three-electrode system containing HEs and AE for the first cycle at scanning rate of $5\ \text{mV s}^{-1}$ (c). CV of $\text{Na}_3\text{V}_2(\text{PO}_4)_3$ working electrode (coated on titanium) in a three-electrodes cell containing HE-3 for the first three cycles from -0.7 V to -1.5 V vs. Ag/AgCl at scanning rate of $5\ \text{mV s}^{-1}$ (d).



hydrogen evolution potentials cannot be distinguished in HE-1 and HE-5, the corresponding Na^+ deintercalation peaks are still distinct, confirming the PAAS effect in Fig. 2. By contrast, the potential of Na^+ intercalation in HE-3 is well distinguishable from that of hydrogen evolution despite their small difference. The symmetric redox peaks at -1.36 V and -1.18 V vs. Ag/AgCl (*i.e.* 1.56 V and 1.74 V vs. Na/Na⁺), accorded with the reported results,^{21–24} demonstrate the reversible sodium-ion intercalation/deintercalation of $\text{Na}_3\text{V}_2(\text{PO}_4)_3$ in HE-3. This result proves that HE-3 effectively broadens the ESW of aqueous electrolyte and allows the reversible Na-ion intercalation/deintercalation of $\text{Na}_3\text{V}_2(\text{PO}_4)_3$ as an anode in aqueous electrolyte.

The electrochemical cycle reversibility of $\text{Na}_3\text{V}_2(\text{PO}_4)_3$ has been further examined by multiple CV test from -0.7 V to -1.5 V (vs. Ag/AgCl). As shown in Fig. 5d, the reduction peaks and oxidation peaks appear at approximately -1.38 V and -1.19 V (vs. Ag/AgCl) respectively for the initial three cycles. These three cycles are highly coincident, reflecting the good Na^+ -intercalation/deintercalation reversibility of $\text{Na}_3\text{V}_2(\text{PO}_4)_3$ electrode in HE-3. In addition, the Na^+ storage capacity of $\text{Na}_3\text{V}_2(\text{PO}_4)_3$ can be estimated from the reversible cyclic voltammetry (CV) curves using the following eqn (1).²⁸

$$C_{\text{NVP}} = \frac{Q}{m} = \frac{It}{m} = \frac{\int IdV}{mv_s} \quad (1)$$

$$m = 0.467 \text{ mg}, v_s = 5 \text{ mV s}^{-1}, \int IdV = 309.793 \text{ mA V}$$

where C_{NVP} and m are the specific capacity and mass of $\text{Na}_3\text{V}_2(\text{PO}_4)_3$ material, Q refers to the quantity of electric charge, which is equal to the product of current (I) and time (t), that is, the ratio of the shaded area ($\int IdV$) under the CV curve to the scan rate (v_s).

The specific capacity of $\text{Na}_3\text{V}_2(\text{PO}_4)_3$ electrode was calculated from CV curves (Fig. 5d) and eqn (1). The specific capacity of $\text{Na}_3\text{V}_2(\text{PO}_4)_3$ electrode is about 37.2 mA h g^{-1} during the reduction process. Although this capacity is lower than the previously reported capacity of $\text{Na}_3\text{V}_2(\text{PO}_4)_3$ in non-aqueous electrolyte (67 mA h g^{-1}),²³ it should be mentioned that the dynamic factors, such as the particle size and scanning rate, could influence the available capacity. The reversible electrode reaction provides the possibility for the research on aqueous $\text{Na}_3\text{V}_2(\text{PO}_4)_3$ -based cells and other aqueous cell systems using an anode that has a lower potential than the frequently used $\text{NaTi}_2(\text{PO}_4)_3$.

Conclusions

We have investigated the PAAS hydrogel electrolyte containing $1 \text{ M Na}_2\text{SO}_4$ for potential use in aqueous Na-ion batteries. It is found that the PAAS content has obvious influence on the hydrogen evolution potential. Adding 3 wt\% PAAS to $1 \text{ M Na}_2\text{SO}_4$ aqueous electrolyte effectively inhibits the hydrogen evolution. The ESW of aqueous gel electrolyte is broadened to an extent of 330 mV from 2.12 V (in AE) to 2.45 V (in HE-3) on

stainless steel current collector, and particularly the hydrogen evolution potential is shifted to -1.75 V vs. Ag/AgCl (*i.e.* 1.17 V vs. Na/Na⁺) on titanium current collector. DFT calculation and spectroscopic analysis confirm the interaction between water molecules and PAAS, which may decrease the water activation. Finally, through CV test and cathodic area calculation we first prove the feasibility of $\text{Na}_3\text{V}_2(\text{PO}_4)_3$ anode for reversible Na storage in this electrolyte with the stable capacity of *ca.* 37.2 mA h g^{-1} .

Experimental

Electrolytes preparation

Aqueous electrolyte (AE, 1 M anhydrous sodium sulfate (Na_2SO_4 , Sinopharm Chemical Reagent Co., Ltd) in deionized water (HPLC grade)) was prepared according to molality (mol-salt in kg-solvent). The hydrogel electrolytes (HEs) were prepared by mixing $1 \text{ M Na}_2\text{SO}_4$ solution with different ratios (1 wt\% , 3 wt\% , 5 wt\% , named HE-1, HE-3, HE-5, respectively) of poly(acrylate sodium) (PAAS, $M_w = 300\text{w}–700\text{w}$, Aladdin), and then followed by intense stirring under room temperature until dissolved.

Material synthesis and electrode preparation

The $\text{Na}_3\text{V}_2(\text{PO}_4)_3$ powder was synthesized by spray drying method as reported, in which a given amount of NH_4VO_3 (99.9% , Macklin), $\text{NH}_4\text{H}_2\text{PO}_4$ (99% , Aladdin), Na_2CO_3 (99% , Energy Chemical) and glucose (as the carbon precursor and the reductive agent) were dissolved in deionized water and stirred at 80°C until blue clear solution formed. The blue solution was spray-dried to obtain the precursor by a spraying dryer (BUCHI Mini Spray Dryer B-290), where the inlet and outlet temperatures were set at 200°C and 105°C , respectively, the feed pump speed was 8% and the gas speed was 5000 mL min^{-1} . Then, the obtained powder was pre-calcined in a tube furnace at 350°C for 5 h and calcined at 750°C for 12 h in N_2 atmosphere. The $\text{Na}_3\text{V}_2(\text{PO}_4)_3$ electrodes were prepared as followed: $\text{Na}_3\text{V}_2(\text{PO}_4)_3$ material, Super P and polyvinylidene fluoride (PVDF) were mixed with a weight ratio of $8 : 1 : 1$ in N -methyl-2-pyrrolidone (NMP), which was spin-coated on a titanium grid, and was dried at 80°C for 8 h under vacuum condition.

Material characterizations

FTIR spectra were measured on a PerkinElmer Spectrum 100. Raman spectra were collected with a DXR Raman Microscope using a 532 nm diode-pumped solid-state laser between 4000 and 2700 cm^{-1} , with all the samples sealed in a glass test tube. The scanning electron microscopy (SEM) images of $\text{Na}_3\text{V}_2(\text{PO}_4)_3$ powder were obtained on Hitachi-X650 microscope (20 kV) scanning electron microscopy. The X-ray diffraction (XRD) patterns were recorded on a scan rate of $2^\circ \cdot \text{min}^{-1}$ from 10° to 65° by using Rigaku diffractometer ($D_{\text{max}}-2200$) with Cu-K radiation. The carbon content in $\text{Na}_3\text{V}_2(\text{PO}_4)_3$ powder was analyzed using a Thermo Gravimetric Analyzer (TGA/Pyris 1 TGA).



Electrochemical measurements

Ionic conductivity was measured with Rex conductivity meter DDS-307 at room temperature. The electrochemical stability windows (ESW) of the electrolytes were examined by cyclic voltammetry (CV) using CHI650C electrochemical workstation and the glassy three-electrode system with Ag/AgCl as reference electrode (2.92 V vs. Na/Na⁺), stainless steel (SS 304), aluminum (Al), titanium (Ti), platinum (Pt) and prepared Na₃V₂(PO₄)₃ as working electrodes, and graphite as counter electrode. The experiments were conducted at scanning rate of 10 or 5 mV s⁻¹ in a given potential range at 25 °C.

Conflicts of interest

There are no conflicts to declare.

Acknowledgements

This work was supported by the National Natural Science Foundation of China (No. 21975158).

Notes and references

- 1 V. Palomares, P. Serras, I. Villaluenga, K. B. Hueso, J. Carretero-González and T. Rojo, *Energy Environ. Sci.*, 2012, **5**, 5884–5901.
- 2 H. Pan, Y.-S. Hu and L. Chen, *Energy Environ. Sci.*, 2013, **6**, 2338–2360.
- 3 K. Xu, *Chem. Rev.*, 2004, **104**, 4303–4418.
- 4 Y. Qiao, X.-L. Hu, Y. Liu and Y.-H. Huang, *Electrochim. Acta*, 2012, **63**, 118–123.
- 5 Y. Huang, L. Zhao, L. Li, M. Xie, F. Wu and R. Chen, *Adv. Mater.*, 2019, **31**, 1808393.
- 6 C. Wessells, R. A. Huggins and Y. Cui, *J. Power Sources*, 2011, **196**, 2884–2888.
- 7 C. Yang, J. Chen, T. Qing, X. Fan, W. Sun, A. Cresce, M. S. Ding, O. Borodin, J. Vatamanu, M. A. Schroeder, N. Eidson, C. Wang and K. Xu, *Joule*, 2017, **1**, 122–132.
- 8 L. Suo, O. Borodin, Y. Wang, X. Rong, W. Sun, X. Fan, S. Xu, M. A. Schroeder, A. V. Cresce, F. Wang, C. Yang, Y.-S. Hu, K. Xu and C. Wang, *Adv. Energy Mater.*, 2017, **7**, 170–189.
- 9 R.-S. Kühnel, D. Reber and C. Battaglia, *ACS Energy Lett.*, 2017, **2**, 2005–2006.
- 10 A. Ponrouch, E. Marchante, M. Courty, J.-M. Tarascon and M. R. Palacin, *Energy Environ. Sci.*, 2012, **5**, 8572–8583.
- 11 H. Li, Y. Wang, H. Na, H. Liu and H. Zhou, *J. Am. Chem. Soc.*, 2009, **131**, 15098–15099.
- 12 C. Deng, S. Zhang, Z. Dong and Y. Shang, *Nano Energy*, 2014, **4**, 49–55.
- 13 W. Li, J. R. Dahn and D. S. Wainwright, *Science*, 1994, **264**, 1115–1118.
- 14 J. Luo, W. Cui, P. He and Y. Xia, *Nat. Chem.*, 2010, **2**, 760–765.
- 15 B. H. Zhang, Y. Liu, Z. Chang, Y. Q. Yang, Z. B. Wen, Y. P. Wu and R. Holze, *J. Power Sources*, 2014, **253**, 98–103.
- 16 Y. Wang, L. Mu, J. Liu, Z. Yang, X. Yu, L. Gu, Y.-S. Hu, H. Li, X.-Q. Yang, L. Chen and X. Huang, *Adv. Energy Mater.*, 2015, **5**, 1501005.
- 17 H. Qin, Z. P. Song, H. Zhan and Y. H. Zhou, *J. Power Sources*, 2014, **249**, 367–372.
- 18 L. Chen, W. Li, Y. Wang, C. Wang and Y. Xia, *RSC Adv.*, 2014, **4**, 25369.
- 19 C. Park, M. Kanduć, R. Chudoba, A. Ronneburg, S. Risse, M. Ballauff and J. Dzubiella, *J. Power Sources*, 2018, **373**, 70–78.
- 20 T. Liu, B. Wang, X. Gu, L. Wang, M. Ling, G. Liu, D. Wang and S. Zhang, *Nano Energy*, 2016, **30**, 756–761.
- 21 Z. Jian, W. Han, X. Lu, H. Yang, Y. Hu, J. Zhou, Z. Zhou, J. Li, W. Chen, D. Chen and L. Chen, *Adv. Energy Mater.*, 2013, **3**, 156.
- 22 W. Song, X. Cao, Z. Wu, J. Chen, K. Huangfu, X. Wang, Y. Huang and X. Ji, *Phys. Chem. Chem. Phys.*, 2014, **16**, 17681–17687.
- 23 W. Duan, Z. Zhu, H. Li, Z. Hu, K. Zhang, F. Cheng and J. Chen, *J. Mater. Chem. A*, 2014, **2**, 8668–8675.
- 24 L. S. Plashnitsa, E. Kobayashi, Y. Noguchi, S. Okada and J.-i. Yamaki, *J. Electrochem. Soc.*, 2010, **157**, A536–A543.
- 25 R. C. Weast, S. M. Selby and C. D. Hodgman, *Angew. Chem., Int. Ed.*, 2010, **5**, 907–908.
- 26 S. Shi, J. Gao, Y. Liu, Y. Zhao, Q. Wu, W. Ju, C. Ouyang and R. Xiao, *Chin. Phys. B*, 2016, **25**, 018212.
- 27 D.-W. Lim, K.-G. Song, K.-J. Yoon and S.-W. Ko, *Eur. Polym. J.*, 2002, **38**, 579–586.
- 28 B. Pandit, D. P. Dubal and B. R. Sankapal, *Electrochim. Acta*, 2017, **242**, 382–389.

